Mineralogical Magazine, December 2008, Vol. 72(6), pp. 1229–1242

Polyhedral serpentine: a spherical analogue of polygonal serpentine?

G. Cressey[1],*, B. A. Cressey[2] and F. J. Wicks[3]

[1] Department of Mineralogy, Natural History Museum, Cromwell Road, London SW7 5BD, UK
[2] Electron Microscopy Centre, School of Chemistry, University of Southampton, Southampton SO17 1BJ, UK
[3] Natural History Department, Royal Ontario Museum, 100 Queen's Park, Toronto M5S 2C6, Canada

[*Received 20 October 2008; Accepted 1 February 2009*]

ABSTRACT

Vugs in late hydrothermal veins in the serpentinite at Gew-graze, Lizard, Cornwall, UK, contain serpentine spheres $\leqslant 0.7$ mm in diameter composed of a crystallographically controlled radial array of well crystallized lizardite-1T crystals. Examinations with optical and scanning electron microscopy reveal that the spheres actually have polyhedral morphology. The polyhedral facets at the sphere surface are the (0001) terminations of individual single crystals of lizardite. Each lizardite crystal is a hexagonal prism and tapers inwards to the core. The angle from prism axis to prism axis is always ~24º, and this angle is consistent even though individual prisms have not maintained contact during growth. The space between prisms is filled by smaller crystals of lizardite in more random orientations, forming a solid sphere. Collectively, the tapering prisms form a growth array that produces a surface tessellation consisting of mainly 6-fold neighbours, but with some 5-fold arrangements to accommodate a closed spherical structure. A 'buckyball', modified by adding face-centring points to each hexagon and pentagon, provides a useful model to describe the space filling adopted by the polyhedral lizardite spheres. Cross sections (close to an equatorial plane) through these polyhedral spheres resemble cross sections of polygonal serpentine, with 15 sectors at 24º to each other, though very much larger in diameter.

Keywords: serpentine, polyhedral, polygonal, Lizard, UK.

Introduction

Spherical or polyhedral serpentine from diverse sources, including meteorites, mid-Atlantic ridge and Alpine serpentinites, has been the subject of several recent detailed studies (Zega *et al*., 2006; Andréani *et al*., 2007; Baronnet *et al*., 2007; Andréani *et al*., 2008), although polyhedral serpentine spheres have been noted in studies of many localities through the years. Crudely circular features that produce black extinction crosses in the petrological microscope have been observed in fracture-filling serpentine veins from many serpentinites (e.g. fig. 7*c* in Wicks and Whittaker, 1977; fig. 12*a*,*b* in Andréani *et al*., 2007; fig. 1*a* in Baronnet *et al*., 2007; fig. 2 in Andréani *et al*., 2008). However, in these occurrences the serpentine spheres are intergrown and when viewed in two-dimensions their spherical nature is not easily recognized nor clearly understood. In contrast, when serpentine spheres have grown in cavities, their spherical nature is more easily recognized. Papp (1988 and pers. comm.) described spherical serpentine in serpentine-altered xenoliths in basalts, and Mitchell and Putnis (1988, figs 5−8), using a Scanning Electron Microscope (SEM), reported globular and colloform structures decorating polygonal serpentine, chrysotile fibres and platy lizardite in kimberlites. Spherulitic serpentine has been noted by Cressey *et al.* (1993) as spherules or radial bundles associated with the Tilly Foster serpentine.

---

* E-mail: g.cressey@nhm.ac.uk
DOI: 10.1180/minmag.2008.072.6.1229

A number of terms have been used to describe these structures; spherical, spheroidal, globular, colloform, polyhedral, radial and onion morphologies. Papp (pers. comm.) first discussed the merits of the terms spherical and polyhedral serpentine. Polyhedral lizardite or polyhedral serpentine has been recommended by Zega *et al.* (2006), Andréani *et al.* (2007) and Baronnet *et al.* (2007). We further endorse the use of the term polyhedral lizardite spheres, or polyhedral serpentine spheres if the serpentine mineral is not known, because it is definitive and emphasizes the relationship of the polyhedral spheres to polygonal serpentine.

Instrumental methods

X-ray powder diffraction (XRD) data were collected using a Nonius PDS120 Powder Diffraction System with a 120º2θ INEL curved position-sensitive detector. Copper-$K\alpha_1$ radiation was selected using a germanium (111) single-crystal monochromator. Silver behenate and Y_2O_3 were used as external 2θ calibration standards and the 2θ linearization of the detector was performed using a least-squares cubic spline function (Cressey and Schofield, 1996; Batchelder and Cressey, 1998). A Stoe Reciprocal Lattice Explorer fitted with a Polaroid camera was used in Buerger Precession mode with Mo-$K\alpha$ radiation for the single-crystal experiments.

Reflected light microscopy was performed using a Zeiss Axioplan microscope fitted with a JVC KY-F70 CCD camera in combination with the image software *Automontage*. Cross-polarized reflected light was used; this produces a clearer, more detailed image of the surface of the polyhedral spheres than plane-polarized reflected light. However, it does impart a yellow-green hue to the images that masks the true pale pink hue of the actual specimens (Fig. 1). Transmitted light microscopy using a Leica DMRX microscope fitted with a JVC KY-F1030 CCD camera was also employed.

The SEM examination was performed using a JEOL JSM 5910 operating at 15 kV, and transmission electron microscopy (TEM) was performed using a JEOL JEM 3010 operating at 300 kV. Chemical analyses were obtained using a Cameca SX50 electron microprobe wavelength-dispersive X-ray spectrometry (WDS) system.

Sample

The lizardite crystals studied are prismatic and occur in radial arrays that form almost perfect polyhedral spheres ⩽0.7 mm diameter (Fig. 1). Each sphere is composed essentially of close-

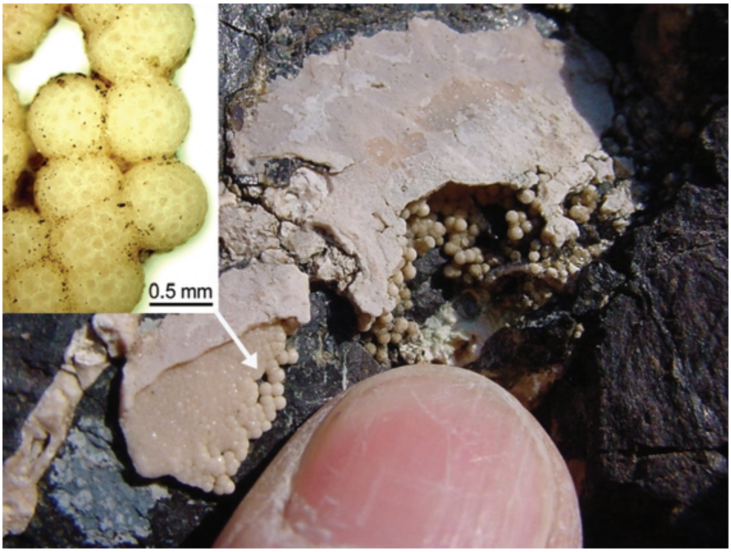

FIG. 1. The lizardite spheres at Gew-graze, lining an exposed vug cavity in the serpentine breccia (finger tip shown for scale). Insert shows the ‘studded’ nature of each sphere surface (optical micrograph in reflected light with crossed polars).

packed individual lizardite crystals with tapering hexagonal prism morphology. The radial array of lizardite prisms is clearly not random, but is a crystallographically controlled growth form.

The spheres occur in late-stage vugs in a hydrothermal lizardite vein-fill in fault-related serpentine breccia from Gew-graze, near Kynance Cove, at the Lizard, Cornwall (Cressey *et al*., 2008). At this locality the lizardite pseudomorphic-textured serpentinite is a dark-red-coloured variety and has been heavily fractured and subsequently cemented by pale-coloured lizardite to form a distinctive matrix-supported breccia. Several different phases of lizardite formation have filled the gaps between the breccia fragments: the earliest appears to be a pale green lizardite that is itself brecciated and re-cemented by a friable pale greenish lizardite in some places and by a pale pinkish compact lizardite in others. The later pinkish spheres of lizardite, the subject of this paper, line vugs in cavities in the breccia (Fig. 1). A pure white compact lizardite crystallized last and fills some of the late openings of the near-vertical fracture system.

X-ray diffraction indicates that these are all lizardite-1*T*. However, the pale green and pure white lizardite have disordered layer stacking ($h0\bar{h}l$ reflections are very weak or absent) and the pinkish compact and spherical lizardites have well ordered layer stacking (distinguished by sharp $h0\bar{h}l$ reflections). X-ray diffraction of a powdered single lizardite sphere produces intense, sharp $h0\bar{h}l$ reflections and its cell parameters refine in space group $P31m(157)$ to $a = 5.3112(6)$ Å, $c = 7.3062(4)$ Å.

Fragments of a hexagonal prism lizardite crystal from a sphere were ground and dispersed onto carbon film for investigation by TEM. Electron diffraction (Fig. 2), with the beam parallel to [0001], exhibits a perfectly sharp hexagonal net with no hint of diffuse satellite streaking (even when the intensity is gamma-stretched) indicating the absence of any buckling or modulation of the flat lizardite structure. Low-magnification TEM images of fragments of these exceptionally large and structurally well formed lizardite crystals show that in addition to the perfect cleavage on {0001}, cleavages of moderate quality also occur on $\{10\bar{1}0\}$ and $\{11\bar{2}0\}$. This is the first reported observation of cleavage forms other than {0001} for lizardite.

Associated pale pinkish crystals with hexagonal platy morphology in interlocking curved aggregates have been described by Cressey *et al*. (2008). These large, flat, structurally well ordered lizardite crystals form curving stacks along [0001], but are otherwise unconstrained. In

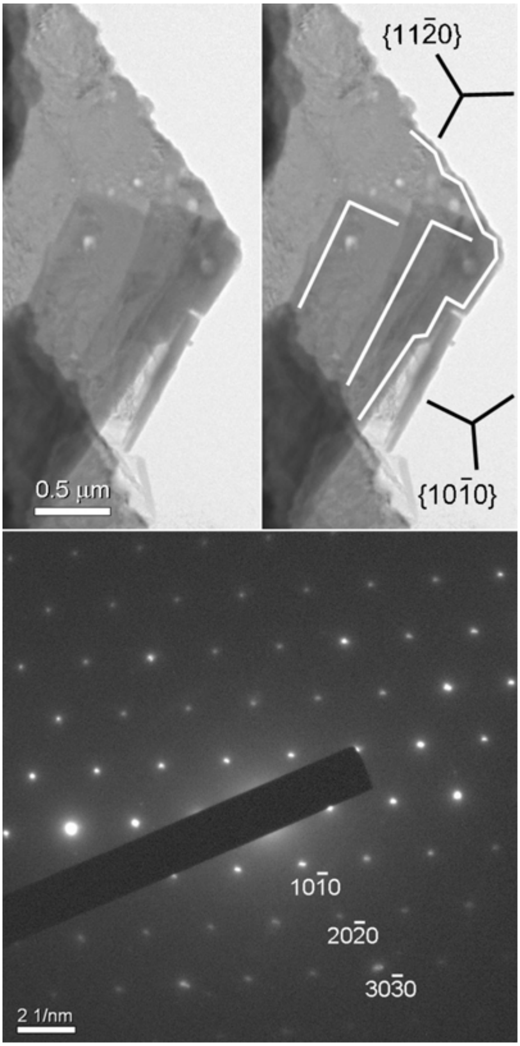

FIG. 2. Electron diffraction pattern recorded with the beam parallel to [0001] of a large fragment of lizardite extracted from a crushed sphere. The diffracted intensity shown has been gamma stretched in order to reveal any weak satellite streaking, but none is apparent indicating the absence of any buckling or modulation of the flat lizardite structure. On the image, $\{10\bar{1}0\}$ and $\{11\bar{2}0\}$ cleavage forms are shown in black, and observed cleavages in white. This crystal fragment exhibits perfect cleavage on {0001} and moderate cleavages on $\{10\bar{1}0\}$ and $\{11\bar{2}0\}$.

comparison, the individual lizardite crystals forming the polyhedral spheres described here are similar in size and perfection to those in the curving stacks, but their arrangement is crystallographically controlled within each sphere.

Rucklidge and Zussman (1965) noted that the type lizardite crystals from the Lizard, Cornwall are often bent into a spherical cap, but this is a different feature from polyhedral lizardite spheres.

Sphere crystal chemistry

Quantitative WDS microprobe analyses, from positions shown in Fig. 3 and listed in Table 1, were collected on an equatorial section through the interior of a sphere. The analyses indicate that these lizardite crystals are exceptionally Mg-rich; on average they contain <0.1 wt.% Fe, <0.1 wt.% Mn, and <0.1 wt.% Al. It is possible that the very minor Mn content gives the lizardite its pinkish hue. Although the Fe, Mn and Al contents are very small, a subtle trend of decreasing Al (and possibly Mn and Fe) from core to rim is apparent for the sphere analysed. The significance of the slightly smaller concentrations of Mg (average = 25.10 wt.%) and Si (average = 19.64 wt.%), which we have reason to believe are real, relative to those expected for $Mg_3Si_2O_5(OH)_4$ (Mg = 26.32 wt.%; Si = 20.27 wt.%), will be discussed in another paper (in preparation). This is essentially an Al-free lizardite-1*T*, providing further evidence that a flat lizardite structure can form without significant Al substitution (Cressey *et al*., 2008).

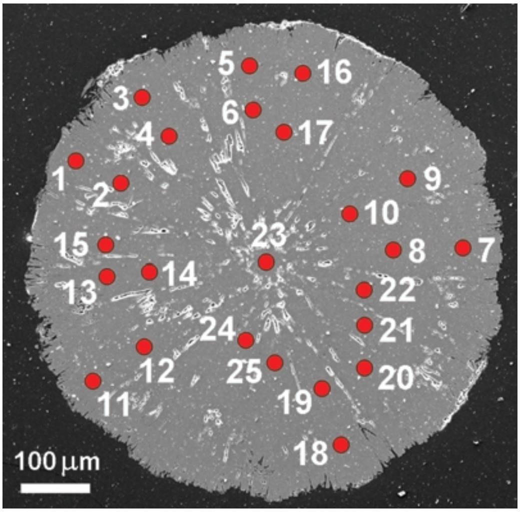

FIG. 3. Secondary electron image of a lizardite sphere cut and polished close to an equatorial plane. The red circles show the locations of the 20 µm diameter electron microprobe spots analysed by WDS. Analysis numbers refer to results shown in Table 1.

Assuming an ideal formula and equal distribution of Al between the octahedral and tetrahedral sites, the average composition (excluding the analysis spot at the core) for this spherical

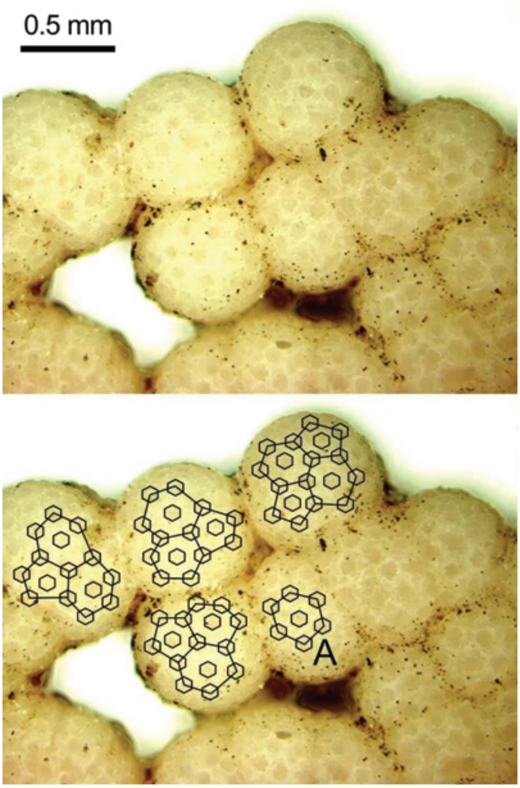

FIG. 4. Optical micrograph of the lizardite spheres recorded in reflected light with crossed polars, showing 'studded' surfaces formed by the (0001) terminations of individual lizardite single crystals. Each lizardite crystal has a tapering hexagonal prism morphology extending radially from the core to the surface of each sphere. Commonly, each crystal termination (represented by a small hexagon) is observed to be surrounded by six others in a hexagonal array, and sometimes by five others in a pentagonal array. Shown below, the partially-constructed network identifies a hexagon-pentagon surface tessellation that approximates to 'face-centred buckyball' geometry. The sphere labelled 'A' is further investigated in Fig. 13. (The black material adhering to the spheres is recent organic debris deposited from water that flowed through the vug).

TABLE 1. Wavelength-dispersive X-ray spectrometry analyses of the interior of a lizardite sphere by electron microprobe.

#	Si	Ti	Al	Cr	Fe	Mn	Mg	Ca	Na	K	O*	Total
1	20.09	n.d.	0.07	n.d.	0.04	0.08	25.70	n.d.	n.d.	n.d.	39.90	85.88
2	20.10	n.d.	0.09	n.d.	0.08	0.08	25.46	n.d.	n.d.	n.d.	39.78	85.59
3	19.98	n.d.	0.06	n.d.	0.07	0.08	25.31	n.d.	n.d.	n.d.	39.52	85.02
4	19.74	n.d.	0.07	n.d.	0.07	0.09	25.10	n.d.	n.d.	n.d.	39.12	84.19
5	19.59	n.d.	0.07	n.d.	0.03	0.09	25.07	n.d.	n.d.	n.d.	38.91	83.76
6	19.70	n.d.	0.09	n.d.	0.07	0.07	25.12	n.d.	n.d.	n.d.	39.10	84.15
7	19.22	n.d.	0.06	n.d.	0.04	0.04	24.85	n.d.	n.d.	n.d.	38.33	82.54
8	19.49	n.d.	0.08	n.d.	0.10	0.08	24.96	n.d.	n.d.	n.d.	38.75	83.46
9	19.40	n.d.	0.08	n.d.	0.09	0.08	24.75	0.02	n.d.	n.d.	38.52	82.94
10	19.49	n.d.	0.09	n.d.	0.14	0.11	24.83	n.d.	n.d.	n.d.	38.70	83.36
11	19.97	n.d.	0.05	n.d.	0.03	0.10	25.30	n.d.	n.d.	n.d.	39.48	84.93
12	19.84	n.d.	0.09	n.d.	0.08	0.09	25.35	n.d.	n.d.	n.d.	39.42	84.87
13	19.96	n.d.	0.08	n.d.	0.09	0.09	25.36	n.d.	n.d.	n.d.	39.55	85.13
14	19.92	n.d.	0.07	n.d.	0.08	0.08	25.14	n.d.	n.d.	n.d.	39.35	84.64
15	19.93	n.d.	0.08	n.d.	0.08	0.08	25.30	n.d.	n.d.	n.d.	39.47	84.94
16	19.49	n.d.	0.08	n.d.	0.02	0.10	24.82	n.d.	n.d.	n.d.	38.65	83.16
17	19.59	n.d.	0.09	n.d.	0.09	0.07	24.99	n.d.	n.d.	n.d.	38.89	83.72
18	19.32	n.d.	0.07	n.d.	0.04	0.08	24.85	n.d.	n.d.	n.d.	38.46	82.82
19	19.31	n.d.	0.07	n.d.	0.07	0.08	25.16	n.d.	n.d.	n.d.	38.66	83.35
20	19.38	n.d.	0.08	n.d.	0.08	0.07	24.95	n.d.	n.d.	n.d.	38.61	83.17
21	19.37	n.d.	0.09	n.d.	0.08	0.09	25.11	n.d.	n.d.	n.d.	38.72	83.46
22	19.40	n.d.	0.09	n.d.	0.09	0.11	24.80	n.d.	n.d.	n.d.	38.56	83.05
23	19.47	n.d.	0.19	n.d.	0.32	0.15	24.42	n.d.	n.d.	n.d.	38.56	83.11
24	19.65	n.d.	0.10	n.d.	0.13	0.11	25.10	n.d.	n.d.	n.d.	39.06	84.15
25	19.52	n.d.	0.08	n.d.	0.10	0.09	25.14	n.d.	n.d.	n.d.	38.91	83.84
Average	19.64		0.08		0.08	0.09	25.08				39.01	84.01
Std dev	0.27		0.03		0.06	0.02	0.27				0.45	0.93
Average†	19.64		0.08		0.07	0.08	25.10				39.03	84.04
Std dev†	0.27		0.01		0.03	0.01	0.24				0.45	0.93

analysis spots as shown in Fig. 2.
All values shown as wt.% elements.
n.d. = not detected
* Oxygen calculated by stoichiometry from cation content (assuming Fe^{2+} and Mn^{2+}).
† Average and standard deviation excluding #23 (sphere core).

lizardite can be expressed as $(Mg_{2.987}Fe_{0.004}Mn_{0.005}Al_{0.004})(Si_{1.996}Al_{0.004})O_5(OH)_4$. This is lower in Fe and Al than the lizardite used in the structure determinations by Mellini and Zanazzi (1987), with composition $(Mg_{2.82}Fe_{0.07}Al_{0.09})(Si_{1.94}Al_{0.06})O_5(OH)_4$, and by Mellini and Viti (1994), with composition $(Mg_{2.74}Fe_{0.16}Al_{0.09})(Si_{1.93}Al_{0.07})O_5(OH)_4$.

Sphere geometry

To the naked eye, the lizardite appears to form almost perfect spheres, (Fig. 1) but using a hand lens reveals that the sphere surfaces are not smooth but appear to be 'studded'. Optical microscopy (Fig. 4) and SEM (Fig. 5) show that the surfaces are actually formed of an array of near-hexagonal polyhedral faces, each being the (0001) termination of an individual prismatic lizardite crystal. Each of these crystals protrudes slightly above the surrounding sphere surface which is made up of an aggregate of fine lizardite plates (Fig. 5). Viewed optically in normal incident light, the single-crystal lizardite terminations are reflective but appear darker than their immediate surroundings because the incident light penetrates deeply into the single crystals (as though they were transparent 'windows'), while light is more strongly scattered by the surrounding matrix of fine crystals.

When disaggregated, the spheres break up into individual tapering hexagonal prismatic single lizardite crystals. A single {0001} cleavage plate from one such prism was mounted on a carbon fibre for precession X-ray photography, and the crystal was found to be bounded by $\{10\bar{1}0\}$. (In space group *P*31*m* {0001} and $\{10\bar{1}0\}$ form a hexagonal prism, while {0001} and $\{11\bar{2}0\}$ form a trigonal prism). This information also allows the relative azimuthal crystallographic orientations of *a* and *b* (orthohexagonal) for each hexagonal prism at the sphere surface to be determined. (Orthohexagonal *b* directions are used thoughout this work in order to relate the structures of polygonal and polyhedral lizardite to the circumferential *b* curvature of chrysotile). Another obvious feature of the arrangement of the hexagonal terminations is that each one is surrounded by six others in most cases, and occasionally by five others (Fig. 4).

An interesting aspect of the lizardite spheres is revealed in sections cut and polished at, or close to, an equatorial plane through a sphere. A set of 30 radial lizardite crystals is seen, for which each successive radial crystal is rotated by ~12º to the previous one (Figs 6 and 7). Based on surface morphology, optical properties and arrangement of adjacent radial lizardite crystals in the equatorial plane, the radial crystals can be divided into two sets with each crystal within a set rotated by ~24º to the adjacent crystal. Each of the two 15-crystal sets is rotated by ~12º to each other to produce the 30-crystal set.

There is evidence that the lizardite crystals close to the centre of each sphere initially form as trigonal prisms (Figs 8, 9 and 10) rather than

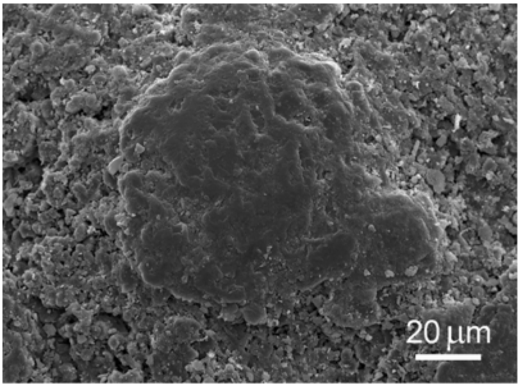

FIG. 5. Each large lizardite crystal protruding from a sphere surface has an approximate hexagonal outline. The volume between the large crystals consists of finer-grained lizardite (secondary-electron image).

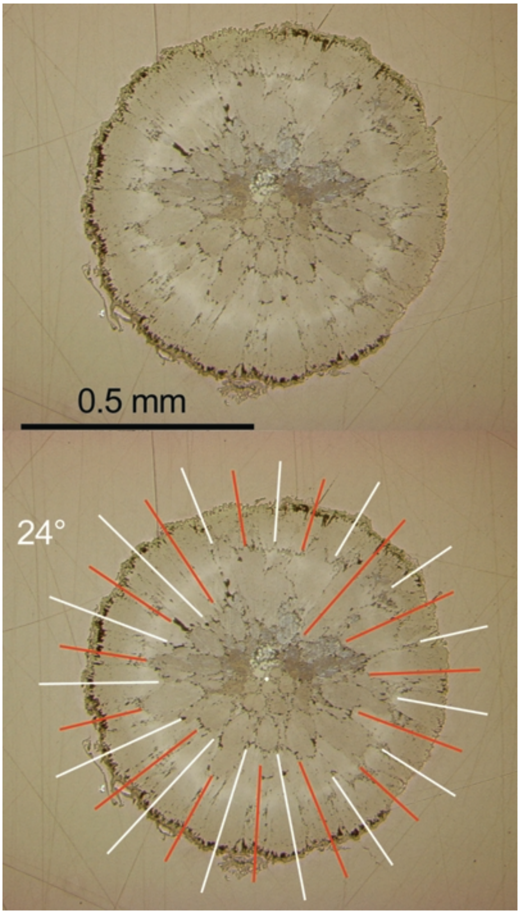

FIG. 6. A polished section though a sphere of lizardite, cut close to an equatorial plane, showing tapering single crystals of lizardite arranged in radial distribution. The nodular appearance at the rim of the sphere results from the lizardite crystals protruding slightly at the surface. This section intersects predominantly one plane of radial crystals (indicated by white lines). Another more oblique plane of crystals is also intersected (red lines). The white and red sets of lines are each drawn radially at 24º apart, and are offset relatively by 12º. Towards the centre of the sphere, parts of other intersecting radial sets of tapering lizardite crystals at more oblique angles are visible. Optical micrograph in plane polarized reflected light.

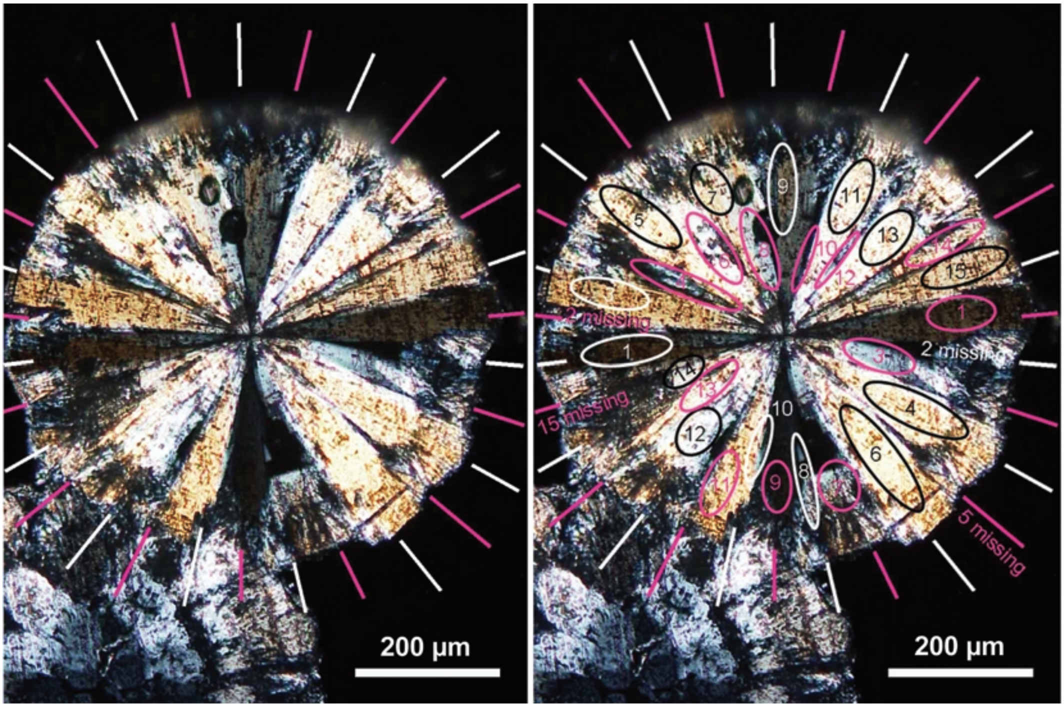

FIG. 7. Optical micrograph in transmitted light with crossed polarizers, of a lizardite sphere embedded in resin and thin-sectioned very close to an equatorial plane. Two 15-fold radial sets of lizardite single crystals are cut by the section (marked white and pink respectively), and their *c* axes are oriented radially in the plane of the section. This pair of planes, offset relatively in azimuth by 12º, together forms an approximate 30-fold polygonal section. At 180º apart, pairs from alternate sets (white and pink) go into extinction as the section is rotated. These 15 pairs are shown numbered; the ellipses indicate the regions that behave optically as single crystals when rotated into extinction. Some sectors (indicated as 'missing') are either not intersected by the section or are composed of fine-grained randomly oriented lizardite crystals.

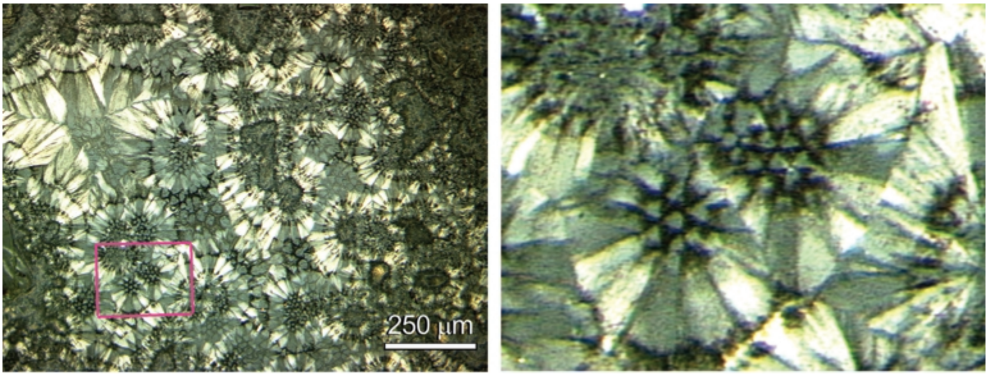

FIG. 8. A polished thin section of an intergrown mass of coalesced polyhedral serpentine viewed in reflected light with crossed polarizers. This consists of well organized radial arrangements of individual tapering trigonal prism crystals of lizardite. Sections through core regions of polyhedra clearly display a crystallographic alignment of the trigonal prisms in three directions at 60º (enlarged area). Trigonal prisms with larger cross sectional area are observed in the interstitial spaces between the near-spherical polyhedra; these are sections of crystals close to polyhedral rims seen in projection.

hexagonal prisms. The trigonal prism morphology appears to be maintained and still apparent at the surface in small spheres, up to ~20–30 µm. These are similar but not identical to the extremely small polygonal spheres, and partial spheres, with triangular faces described by Zega *et al.* (2006), Andréani *et al.* (2007), Baronnet *et al.* (2007) and Andréani *et al*. (2008). However, in the larger spheres formed in cavities at Gew-graze, the individual trigonal prisms at their cores gradually transform into hexagonal prisms outwards towards the surface as they increase in cross-sectional area (Fig. 10). The trigonal prisms at sphere cores are aligned in three planes at ~60º (Fig. 9) and are separated by ~24º to each other in each of these three planes (Fig. 10). In accordance with Baronnet *et al*. (2007), the orientations of the

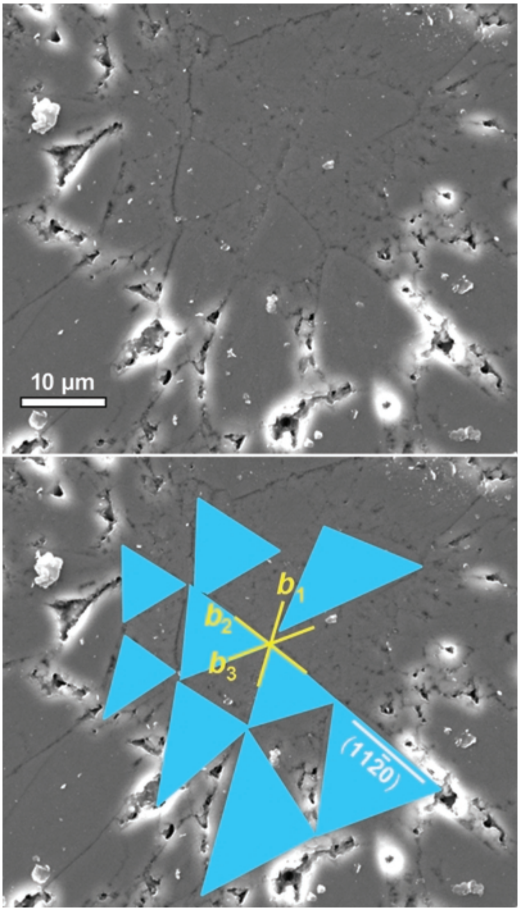

FIG. 9. A secondary electron image from a polished section showing the core region of the sphere in Fig. 3. The sphere core consists of an array of trigonal prisms oriented in three directions at 60º to each other. The triangular spaces between them have been filled with fine-grained lizardite whose grain boundaries are slightly pitted and accentuated by the polishing process. The trigonal single crystals take a better polish and their locations are shown by the blue overlay motif. The central upper region of this image corresponds with the position of the 20 µm electron microprobe analysis spot #23 (see Fig. 3). The activated volume of this spot includes both single crystals and infill components; it also has the largest Al, Mn and Fe (Table 1) relative to the single crystals analysed at all other positions of the sphere.

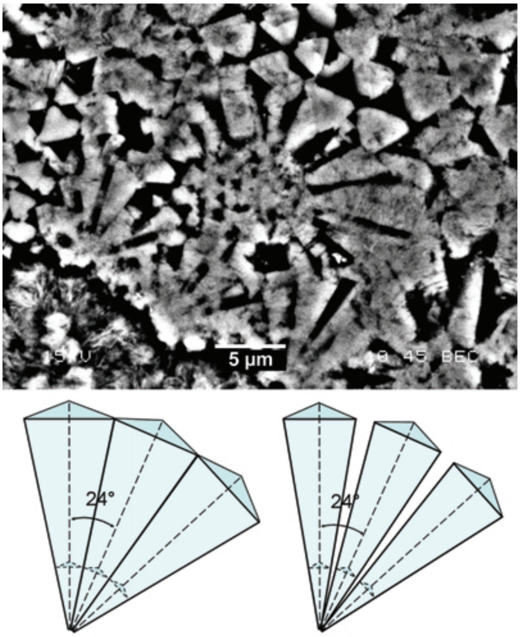

FIG. 10. Backscattered electron image from a polished section of polyhedral serpentine. Radial growths have nucleated at specific points; these consist of trigonal prisms of lizardite oriented at 24º to each other, interpreted as evidence for radial 15-fold nucleation. The triangular cross-sections increase in area as growth proceeds along [0001]. Note the curved outlines and bevelling indicative of the small development of $\{10\bar{1}0\}$ in addition to the dominant $\{11\bar{2}0\}$. The set of trigonal crystals seen end-on (at the top of the image), are all aligned with their orthohexagonal *b* axes in three directions at 60º to each other; these directions run parallel to the alignment of the edges of the triangles. The schematic diagrams show tapering trigonal prisms at 24º to each other in planar arrangements; the angle 24º is consistent even if individual prisms have not maintained growth contact.

triangular faces are taken to be parallel to each of the three equivalent *b*-axis directions, and therefore the trigonal prisms are bounded by $\{11\bar{2}0\}$. Seen in the SEM (Figs 9 and 10), cross sections of the trigonal prisms exhibit 'curved' outlines and bevelling consistent with small developments of $\{10\bar{1}0\}$ in addition to $\{11\bar{2}0\}$. In the outer regions of the spheres, $\{10\bar{1}0\}$ appears to develop in preference producing a near-hexagonal morphology.

The space between the lizardite prisms varies from minor to substantial depending on the relative growth width and attitude of the adjacent prisms. The inter-prism material is solid with some porosity, and composed of smaller plates of lizardite in more varied orientations (Fig. 5). These smaller plates have nucleated on the edges of the large hexagonal prisms, but away from the prisms, unconstrained growth of a mass of smaller lizardite crystals appears to have taken place. Near the outer margin of the spheres, somewhat larger lizardite crystals may nucleate on and grow out at ~30º to the main lizardite prisms (Fig. 11). Crystal growth at the ends of the large lizardite prisms reveals the style of the growth; small tapered prisms nucleate at separate points on (0001), but with their *c* axes parallel. As growth proceeds, these prisms widen and appear to coalesce coherently, often leaving small wedge-shaped voids within the single crystal prism (Fig. 11).

Sphere interpretation

When a surface tessellation network is constructed on each sphere surface (Fig. 4), it becomes clear that the arrangement of the hexagonal prism terminations form a continuous spherical surface that closely approximates the geometry of C_{60} buckminsterfullerine (Kroto *et al.*, 1985). Although the lizardite spheres are not 'buckyballs' *senso stricto*, the geometry and symmetry of a buckyball can be used to interpret the geometry of the packing of lizardite prisms that form a sphere in the same way that an imaginary lattice is used to interpret a crystal structure. However, the buckyball model we propose must first be modified by adding centring points to each hexagon and each pentagon (Fig. 12). Such a face-centred buckyball consists of 92 surface nodes rather than the 60 of a regular buckyball. This idealized spherical geometry provides a model with which to describe and understand the observed growth form of polyhedral lizardite spheres. For this ideal construction, polyhedral lizardite would consist of 92 [0001] prisms (tapering inwards from surface to core) filling the volume with 6- and 5-fold arrays of [0001] prisms.

In this idealized face-centred buckyball model there are 12 circles occurring in pairs; circles in each pair are close and parallel to one another, but lie on opposite sides of an equatorial circle. (Fig. 12). Each circle consists of 15 nodes around its circumference with the nodes 24º apart. At each hexagon of the buckyball, three sets of the paired circles intersect at 60º to each other. Part of this geometrical arrangement is shown mapped

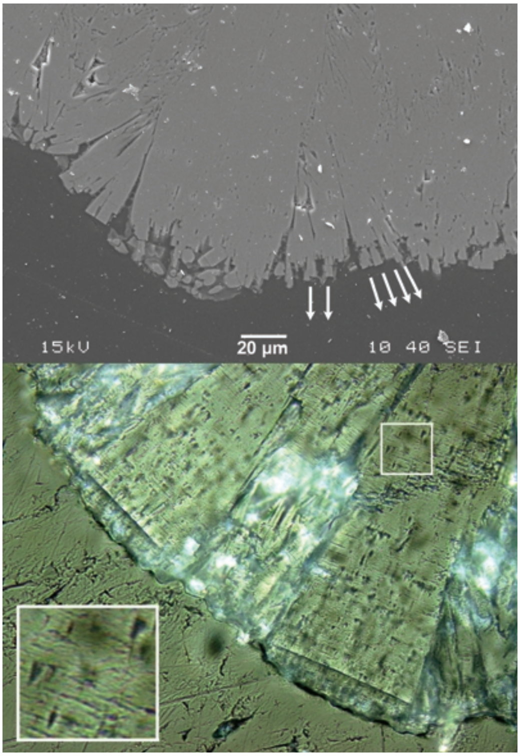

FIG. 11. Secondary electron image (top) and optical image in crossed polarized light (bottom) from a polished section of the outer rims of two spheres, showing adjacent lizardite single-crystal prisms. Inter-prism regions are filled with smaller lizardite crystals and towards the edges of the sphere with larger crystals grown at ~30º to the main prisms. At the growth surface, small tapered lizardite prisms grow with their *c* axes near-parallel (white arrows); as they coalesce, elongated triangular-shaped voids often remain within the large single crystals (enlarged inset).

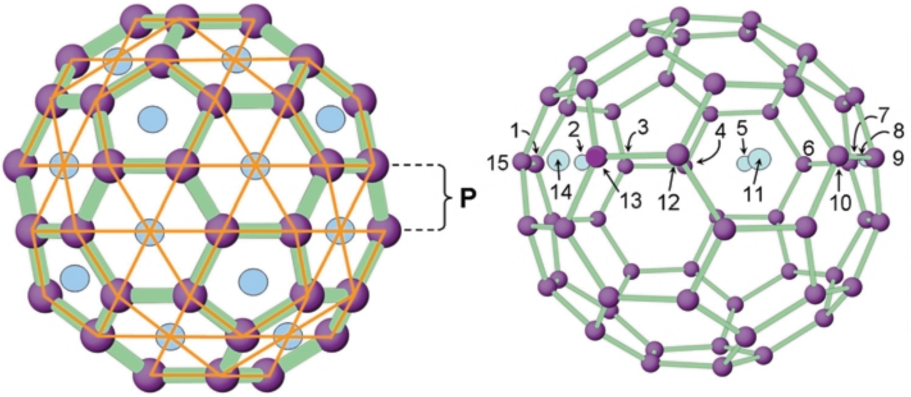

FIG. 12. The surface geometry of a face-centred buckyball, constructed by adding centring points (blue) to each hexagon and pentagon; this produces 92 (rather than 60) surface nodes. This arrangement produces 12 surface circles (shown in orange) each with 15 nodes around their circumference at 24º apart. These 12 circles occur in six pairs that pass just either side of an equatorial great circle. One such pair is labelled 'P'. The two 15-node circles in each pair are offset azimuthally by 12º, forming a 30-node zig-zag arrangement. A single 15-node ring is shown numbered in the perspective view (right).

onto an observed lizardite polyhedron surface in Fig. 13: the centres of the hexagonal lizardite plates, forming the nodes, conform closely to this geometry, and therefore sections in specific directions close to a diameter of the 'sphere' will contain ~15 *c*-axis prisms at 24º to each other. The number 15 is significant if this polyhedral lizardite forms in a similar way, at the nucleation stage, to that of the well known 15-sectored polygonal serpentine (Cressey and

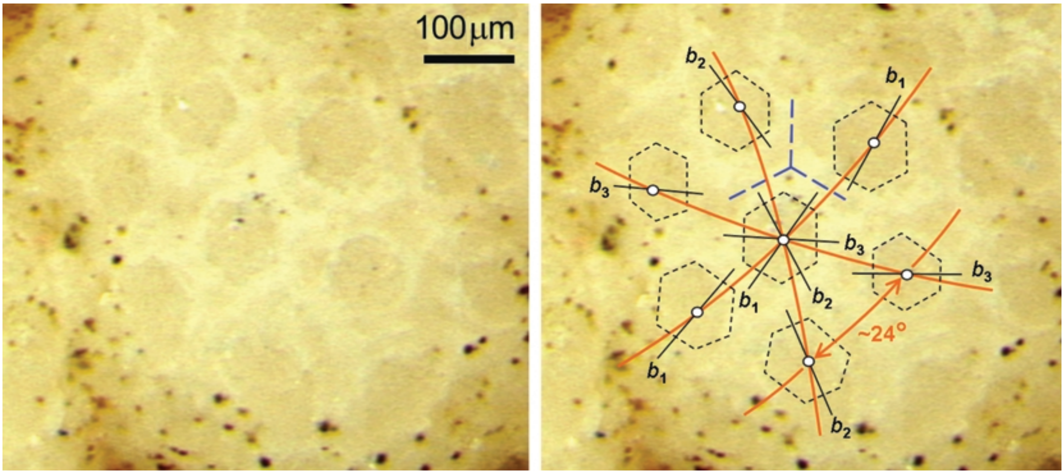

FIG. 13. A view of part of the sphere labelled 'A' in Fig. 4, showing the near-hexagonal shapes of the (0001) faces of individual lizardite crystals. Based on the X-ray precession experiment with a hexagonal plate extracted from the surface of a similar sphere, the hexagonal morphology of these lizardite-1*T* crystals is produced by $\{10\bar{1}0\}$, and this information allows the orientation of each orthohexagonal *b* axis to be plotted (b_1,b_2,b_3). The *c* axes of adjacent hexagonal prisms shown are oriented at ~24º apart and lie on a series of arcs (orange curves) that intersect at 60º. Each hexagon is rotated slightly anticlockwise relative to the alignment of the arc directions. The blue dotted lines indicate where contact between hexagonal units could have been, if they had not grown apart during the sphere formation; the intervening space is filled by fine-grained lizardite.

Zussman, 1976; Baronnet and Devouard, 2005). The orientations of the orthohexagonal *b* axes of each hexagonal plate (determined from the precession experiment) are also shown in Fig. 13: these are close to being tangential to the 15-node circles (as in polygonal serpentine). The hexagonal prisms may have been joined *via* a sector boundary initially, but subsequently have failed to maintain continuity across their boundaries, a likely consequence considering their extensive growth to such unusually large crystal dimensions for lizardite. However, individual [0001] growth directions, oriented at 24º to each other, in 15-fold sets in specific planes, appear to have been established early in their formation and maintained fairly closely throughout growth of the sphere. Interestingly, the orthohexagonal *b*-axes shown in Fig. 13 are all rotated by a small angle in an anticlockwise sense relative to the alignment of the 15-node circles. This rotation is probably the result of a gradual twist that occurred along the [0001] growth direction of each lizardite crystal as the sphere developed.

The 12 surface circles (in six pairs), each containing 15 nodes in the ideal face-centred-buckyball (Fig. 12), represent the sets of terminations of the hexagonal lizardite prisms. In the solid sphere each prism extends to the sphere centre, so that these 15-node planes are actually small-vertex cones (of solid angle ~160º). A pair of such cones is shown in Fig. 14. In projection, these two 15-node cones are rotated by 12º to one another.

This aspect of orientation geometry has been observed in sections of the polyhedral lizardite cut and polished close to an equatorial plane illustrated in Figs 6 and 7 in which two sets of 15-fold arrangements of radial lizardite crystals are seen to be rotated by ~12º to each other.

Discussion

A comparison of the large Gew-graze polyhedral lizardite spheres with the smaller spheres described by Zega *et al.* (2006), Andréani *et al.* (2007), Baronnet, *et al.* (2007) and Andréani *et al.* (2008) shows that not only do the spheres occur over a range of sizes, but also that the growth features change with increasing size. They also reported that the smallest spheres range from tens of nm to several µm in size. The intermediate spheres are ~250 µm in diameter (Figs 8–10), and the largest spheres range up to 0.7 mm (Figs 1, 3 and 4). Each size has slightly different growth features.

At the surface, the smallest spheres (or spheroids) are made up of two sets of equilateral trigonal prisms pointing in opposite directions. An important feature is that continuous curved growth occurs across the boundaries between adjacent prisms (Baronnet *et al.*, 2007, fig. 2*b*). Baronnet *et al.* (2007) estimated that a complete sphere would contain 160 to 180 trigonal prisms. The use of our face-centered buckyball model suggests 184 would be required. As Baronnet *et al.* (2007) have demonstrated in their fig. 3, it is not possible to build the surface of a sphere out of equilateral triangles; consequently surface irregularities and imperfections are regular features of the small spheres, and many appear as slightly flattened domes and partial spherical forms.

In contrast, our intermediate-sized spheres (Figs 8–10) would, in accord with a face-centred buckyball model, be composed of 92 equilateral triangular prisms, i.e. half the number found by Baronnet *et al.* (2007) in the smallest spheres. It appears that one set of trigonal prisms has stopped forming and the space is filled with a fine-grained multitude of lizardite crystals and not single crystals (Fig. 9). Obviously, in the nm-size

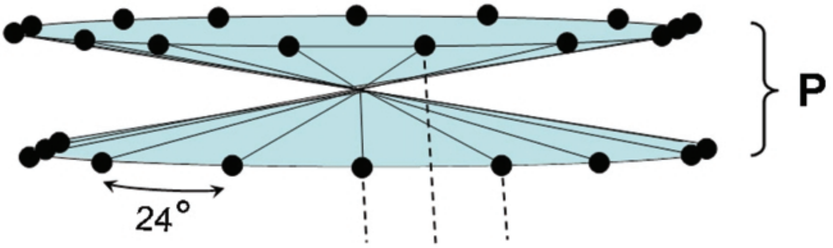

FIG. 14. A pair of 15-node surface circles, extracted from the face-centred buckyball model for pair 'P' shown in Fig. 12. In projection to the sphere centre these form a pair of small height cones, offset in azimuth by 12º and together form a 30-node zig-zag arrangement.

spheres, lizardite can accommodate the strain produced by the spherical nucleation. Baronnet *et al.* (2007) have suggested that the growth across the boundaries between trigonal prisms is made possible by small-angle tilting and/or curvature of faces. However, at some point the strain must be too great and one set of prisms prevails over the other set. It is interesting to note that, in figs 1*c* and 1*d* of Baronnet *et al*. (2007), alternate adjacent triangular faces appear slightly concave, and these could be interpreted as slower growth due to strain, while the other set of triangular faces, reported by Baronnet *et al* (2007) to occur at 24º orientations to each other, form part of a 15-fold ring.

The images of intermediate-sized spheres suggest that the trigonal prisms are beginning to change into hexagonal prisms in this size range (Figs 8 and 10). However, the 24º angle between adjacent prisms is maintained although the prisms are generally not in contact with one another.

The large lizardite spheres are composed of tapered hexagonal prisms that are laterally detached from one another, although still attached at the core. The lack of lateral attachment means that a sphere can form completely composed of hexagonal prisms without having to force pentagonal prism morphologies, as would occur in a buckyball geometry, except by accidental contact during growth.

The use of the face-centred buckyball to interpret the arrangement of the large spheres highlights the connection between polyhedral spheres and polygonal serpentine. Clearly a 15-fold nucleation process occurs in the formation of the polyhedral spheres, is established early in their growth, and is preserved in each core region. The orthohexagonal *b* axes are oriented tangentially around the circular 15-fold arrays of lizardite prisms; this is in the same orientation as that already established for polygonal serpentine (Cressey and Zussman, 1976; Baronnet and Devouard, 2005). Polygonal serpentine forms fibres composed of lizardite crystals arranged in 15 sectors; seen in cross section each of the 15 sectors has *c* radial, *b* (orthohexagonal) tangential, and *a* is the fibre axis. Some polygonal fibres are observed to have a core of cylindrical chrysotile; this may be one way that a 15-fold arrangement of flat lizardite layers could be controlled at an early stage, and is likely to be related to the 5-fold symmetry possessed by chrysotile (Cressey and Whittaker, 1993). As demonstrated by these authors, hydrogen bonding is disordered between successive curved layers of chrysotile except for an in-register radial alignment of the hydrogen bonding 15 times around the circumference arising from the *b*/3 repeat of the hydroxyl sheet between successive layers. At a certain diameter, nucleation from curved chrysotile layers will assume the flat layer morphology of lizardite and generate 15 prisms. In some cases, the original chrysotile nucleation structure could be modified by re-crystallization; this could be the reason why polygonal lizardite is often observed to contain no visible chrysotile core.

For a nucleation event consisting of a few layers of serpentine of small area and for a trigonal (1*T*) structure with three crystallographically equivalent orthohexagonal *b* directions at 0, +60º and −60º, curvature could occur along any one of the *b* directions. For the commonly observed polygonal fibrous serpentine, the normal progression appears to develop only one curvature direction and produce a fibre growing with its axis parallel to *a*. However, if for some reason the *a* fibre direction did not grow to any significant degree (allowing the development of a 15-sectored disc rather than a fibre), then the other curvature options at ±60º to the initial *b* could occur outwards from the 15 positions where the hydrogen bonding is already set in register, generating potentially new sets of 15-node rings. If this ±60º directional curvature occurs repeatedly at each node formed, then the space-filling may begin to form an equidimensional, approximately spherical form. This model for nucleation and growth based on an underlying 5-fold symmetry, producing near-planar 15-fold arrays of lizardite crystals at ±60º to each other forms the basic spherical structure consisting of six pairs of 15-node rings. However, this does not account for the nucleation at the 12 pentagonal sites of the sphere. Prisms at these sites must nucleate at 24º from the structure of one near-neighbour node position in an already-established 15-node ring.

At the sphere surfaces, hexagonal prisms are arranged in 6-, and 5-membered arrays (Fig. 4), but the most common arrangement is a 6-membered grouping that must have been established and set at an early stage, initially as trigonal prisms that developed during growth into free-standing hexagonal prisms.

The angular arrangement of 24º between adjacent sectors in polyhedral lizardite is clearly the result of a nucleation-driven phenomenon similar to that producing the 15 sectors in polygonal serpentine. It is interesting to speculate that polygonal serpentine may result from an early and massive increase in growth preferentially along one of the *a* axes producing fibres from a sectored nucleus disc that could otherwise develop into a sphere. Similarly, it may follow that 30-sectored polygonal serpentine originates when fast growth along one *a* axis coalesces a parallel pair of 15-sectored discs offset azimuthally by 12º in an early, part-formed, sphere. Figure 6 in Andréani *et al* (2008) may provide some evidence for such a sphere-fibre growth mechanism: this figure displays abnormally short polygonal serpentine with bending at the fibre tip perpendicular to the wrapping direction that could be interpreted as a common growth interface between polygonal and polyhedral serpentine.

Conclusions

(1) Spherical polyhedral lizardite is the first mineral growth form observed to develop with a face-centred buckyball symmetry; this is a consequence of both structures possessing a 15-node ring geometry.

(2) Polyhedral lizardite spheres range from nm to mm in size, with a change in morphology from trigonal to hexagonal prisms with increasing size.

(3) It is possible that polyhedral serpentine may occur more commonly than hitherto realized. Now that they have been recognized and analysed, polyhedral lizardite spheres are likely to be reported as a common occurrence of lizardite just as polygonal serpentine was thought to be a rarity and is now recognized as a common form of serpentine. As pointed out by Andréani *et al*. (2008), the general lack of polyhedral serpentine reported in serpentinite studies probably results from its confusion with polygonal serpentine when seen in cross-section by petrographic and transmission electron microscopy. Of the many polygonal-sectored structures that have been seen in TEM images and assumed to be cross sections of polygonal fibres, perhaps some might actually be sections of spherical polyhedral lizardite. The converse may also apply (e.g. Zega *et al.*, 2006, fig, 2*c*); one of the structures is reported to be a section through a polyhedral sphere, but with its elongate chrysotile-like hole at its centre looks very similar to a section of polygonal serpentine.

(4) Polyhedral lizardite spheres and polygonal serpentine are closely related to each other. The lizardite sectors that form both are only different in the way they have been able to grow.

Acknowledgements

FJW thanks the Natural Sciences and Engineering Reseach Council of Canada (NSERC) for the financial support that has made participation in this study possible. The authors are grateful to Marcello Mellini and Peter Bayliss for their constructive comments in the reviews of this paper.

References

Andréani, M., Mével, C., Boullier, A.-M. and Escartin, J. (2007) Dynamic control on serpentine crystallization in veins: Constraints on hydration processes in oceanic peridotites. *Geochemistry Geophysics Geosystems*, **8**, Q02012,doi:10.1029/2006GC001373.

Andréani, M., Grauby, O., Baronnet, A. and Muñoz, M. (2008) Occurrence, composition and growth of polyhedral serpentine. *European Journal of Mineralogy*, **20**, 159–171.

Baronnet, A. and Devouard, B. (2005) Microstructures of common polygonal serpentines from axial HRTEM imaging, electron diffraction and lattice-simulation data. *The Canadian Mineralogist*, **43**, 513–542.

Baronnet, A., Andréani, M., Grauby, O., Devouard, B., Nitsche, S. and Chaudanson, D. (2007) Onion morphology and microstructure of polyhedral serpentine. *American Mineralogist*, **92**, 687–690.

Batchelder, M. and Cressey, G. (1998) Rapid accurate phase quantification of clay-bearing samples using a position-sensitive X-ray detector. *Clays and Clay Minerals*, **46**, 183–194.

Cressey, G. and Schofield, P.F. (1996) Rapid whole-pattern profile stripping method for the quantification of multiphase samples. *Powder Diffraction*, **11**, 35–39.

Cressey, B.A. and Whittaker, E.J.W. (1993) Five-fold symmetry in chrysotile asbestos revealed by transmission electron microscopy. *Mineralogical Magazine*, **57**, 729–732.

Cressey, B.A. and Zussman, J. (1976) Electron microscopic studies of serpentinites. *The Canadian Mineralogist*, **14**, 307–313.

Cressey, G., Spratt, J. and Cressey, B.A. (1993) Electron and X-ray petrography of an unusual serpentine from the Tilly Foster mine, Brewster, New York. *The Canadian Mineralogist*, **31**, 447–458.

Cressey, G., Cressey, B.A. and Wicks, F.J. (2008) The significance of the aluminium content of a lizardite at the nanoscale: the role of clinochlore as an aluminium sink. *Mineralogical Magazine*, **72**, 817–825.

Kroto, H.W., Heath, J.R., O'Brien, S., Curl, R.F. and

Smalley, R.E. (1985) C_{60}: Buckminsterfullerene. *Nature*, **318**, 162–163.

Mellini, M. and Viti, C. (1994) Crystal structure of lizardite-1*T* from Elba, Italy. *American Mineralogist*, **79**, 1194–1198.

Mellini, M. and Zanazzi, P.F. (1987) Crystal structure of lizardite-1*T* and lizardite-2*H* from Coli, Italy. *American Mineralogist*, **72**, 943–948.

Mitchell, R.H. and Putnis, A. (1988) Polygonal serpentine in segregation-textured kimberlite. *The Canadian Mineralogist*, **26**, 991–997.

Papp, G. (1988) *Mineralogical study of serpentines with special regard to the occurrences in Hungary*. PhD thesis, Library of Eőtvős Loránd University, Budapest (in Hungarian).

Rucklidge, J.C. and Zussman, J. (1965) Crystal structure of serpentine mineral lizardite $Mg_3Si_2O_5(OH)_4$. *Acta Crystallographica*, **19**, 381–389.

Wicks, F.J. and Whittaker, E.J.W. (1977) Serpentine textures and serpentinization. *The Canadian Mineralogist*, **15**, 459–488.

Zega, T.J., Garvie, L.A.J., Dodony, I., Friedrich. H., Stroud, R.M. and Buseck, P.R. (2006) Polyhedral serpentine grains in CM chondrites. *Meteoritics and Planetary Science*, **41**, 681–690.